Seismic anisotropy and mantle flow beneath northeast China inferred from regional seismic networks

Juan Li[1,2] and Fenglin Niu[2]

Received 13 February 2010; revised 1 July 2010; accepted 25 August 2010; published 29 December 2010.

[1] Northeast China is situated partly on the Sino-Korean craton and partly on a portion of the Inner Mongolia fold belt. Characterized by widespread Cenozoic intraplate volcanism and deformation caused by multiepisode extension, northeast China is an ideal place to study the underlying physical processes of rifting and active magmatism. We measured SKS wave splitting parameters from several regional networks of broadband stations recently deployed in northeast China. We employed a multievent signal-to-noise ratio (SNR) weighted method and obtained measurements of splitting parameters at 108 stations. These stations cover a variety of tectonic terranes, including the Songliao basin, the Jiamusi massif, the Inner Mongolia belt and the Yanshanian orogenic belt. Overall, the observed SKS splitting times are of low amplitude (~0.8 s), indicating that the underlying mantle experienced relatively weak deformation in this region. The observed anisotropy varies consistently from place to place and exhibits an asymmetric pattern across the Songliao basin. At the southeast edge of the Songliao basin, the fast axis aligns nicely along the NW–SE direction, whereas the axis rotates slightly to NNW toward north beneath the Jiamusi massif. At the west edge of the basin where the north-south gravity lineament (NSGL) is located, we found significant scatter in the fast-axis direction. At the Yanshanian orogenic belt in the southwest corner of the basin, the fast axis aligns along the EW direction. The amplitude of the splitting time appears to be positively correlated with lithospheric thickness, suggesting that lithospheric deformation is the likely cause of the observed seismic anisotropy.

Citation: Li, J., and F. Niu (2010), Seismic anisotropy and mantle flow beneath northeast China inferred from regional seismic networks, *J. Geophys. Res.*, *115*, B12327, doi:10.1029/2010JB007470.

1. Introduction

[2] Northeast China, bounded by the Sino-Korean craton to the south and the subducting west Pacific plate to the east, is an ideal place to investigate subduction processes related to deep earthquakes as well as intraplate volcanism. As an Andean-type margin, northeast China was an elevated plateau formed during the contractional Yanshanian orogeny in the late Jurassic. Mantle derived magmatism was most prominent in northeast China, forming three linearly distributed volcanic belts: Great Xing'an Range, Lesser Xing'an Range and Changbaishan (Figure 1). In Holocene time alkali basalts have erupted in the Changbaishan near the North Korea border as well as in the Lesser Xing'an Range (Figure 1). The rift and extension beginning from the late Jurassic to earlier Cretaceous led to the development of the Songliao basin [*Tian et al.*, 1992], which is bounded by the two volcanically active regions. The mechanisms of the extension and the intraplate volcanism, however, remain poorly understood. Numerous different models have been proposed to address the underlying physical processes related to these issues. Some consider the Holocene volcanic activity to be related to continental marginal arcs [e.g., *Wang*, 1986]; some studies proposed that both asthenospheric upwelling and interactions of Eurasia-Pacific and Eurasia-India plates caused the intracontinental rifting [*Ren et al.*, 2002]. On the basis of the seismic tomography image of a long-stagnant slab under East Asia, *Zhao et al.* [2007a] proposed a big-mantle-wedge model to account for the regional volcanism. *Niu* [2005] suggested that an upward mantle flow induced by lithospheric thinning caused decompression melting and volcanism at the Great Xing'an Range.

[3] Seismic anisotropy provides essential information about the style and geometry of mantle deformation. Seismic waves in an anisotropic media travel at different speeds depending on their propagation and polarization directions. In the upper mantle, it is generally believed that seismic anisotropy is caused by a preferred orientation of olivine crystals, one of the main and the most anisotropic upper mantle minerals. Under dry, relatively high strain rate and simple shear conditions, the olivine a-axis (the seismically

[1]Key Laboratory of the Earth's Deep Interior, Institute of Geology and Geophysics, Chinese Academy of Sciences, Beijing, China.
[2]Department of Earth Science, Rice University, Houston, Texas, USA.

Copyright 2010 by the American Geophysical Union.
0148-0227/10/2010JB007470

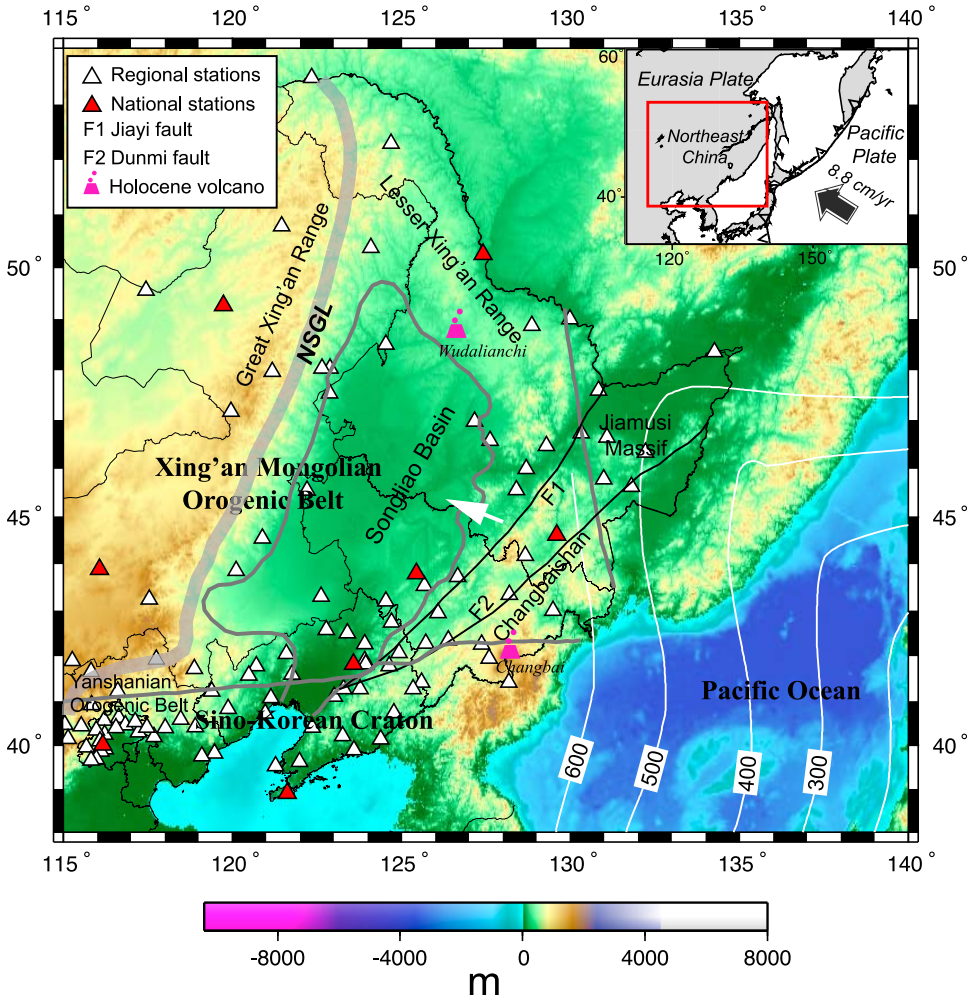

Figure 1. Map showing major faults and tectonic units. Red and white triangles indicate stations associated with Chinese national and regional seismic networks, respectively. NSGL (North South Gravity Lineament) is a 50–100 km transition zone between the Songliao basin and the Inner Mongolia-Xing'an orogenic belt. Faults F1 and F2 are the two branches of the Tanlu fault. The white arrow indicates the absolute plate motion of the studied region with a velocity of 2.0 cm/a. The upper-right insect shows the motion of the Pacific plate relative to the Eurasia plate.

fast axis) aligns roughly parallel to the direction of mantle flow [*Zhang and Karato*, 1995]. The close relationship of finite strain and seismic anisotropy thus can be used to map mantle deformation and ultimately to discriminate between past frozen-in or present mantle flow associated with a wide range of tectonic processes.

[4] Measuring shear wave splitting, or birefringence is one of the most effective methods to characterize seismic anisotropy in the earth's upper mantle [*Silver*, 1996; *Savage*, 1999]. The polarization direction of the fast shear wave φ and the delay time δt between the arrival time of fast and slow wavelets reflect the path-integrated effects of the upper mantle anisotropy. The polarization of the fast split shear wave is primarily controlled by the orientation of the olivine [100] axis which aligns parallel to the flow directions, while the delay time reflects the thickness of the anisotropic layer, the orientation of the ray with respect to the intrinsic anisotropy direction, and the extent of vertical coherence of mantle fabric. Shear wave splitting parameters have been measured over different tectonic environments, e.g., stable continental interiors, subduction zones, rift and extensional regions, which confirmed many predictions of mantle flow by plate tectonics. Complexity of seismic anisotropy, however, has also been revealed with the accumulation of data: trench-parallel and trench-perpendicular fast directions are both observed [e.g., *Fischer et al.*, 1998; *Smith et al.*, 2001; *Baccheschi et al.*, 2007], and 3-D mantle flows associated with variation in slab geometry [*Kneller and van Keken*, 2007] or B-type olivine fabric [*Long and van der Hilst*, 2006] were invoked to interpret different observations.

[5] With the increasing volume of data and improvement in processing technique, a horizontally lying subducting slab has been mapped beneath northeast China [*Huang and Zhao*, 2006], as well as detailed topography of the upper-lower mantle boundary [*Ai et al.*, 2003; *Li et al.*, 2008]. Mantle deformation, which is important to our understanding of the evolution of the North China Craton and the widespread intraplate volcanoes, however, remains ambiguous.

Anisotropic structures beneath northeast China estimated from sparse observations show inconsistent patterns: mantle flow inferred from seismic anisotropy appears to follow neither the direction of plate motion nor local tectonic structure. *Iidaka and Niu* [2001] examined SKS waveform data recorded at China Digital Seismogram Network (CDSN) stations and suggested that the measured fast direction can be best explained by mantle flow induced by the subducting Pacific plate beneath northeast China. *Liu et al.* [2008], on the other hand, found that seismic anisotropy observed at MDJ, a CDSN station right above the front edge of the subducting Pacific slab, originates from the mantle transition zone that might be associated with preferred alignment of metastable olivine within the subducted Pacific plate. The very limited number of CDSN stations appears to be far from sufficient to evaluate these different ideas.

[6] In this study we present the SKS splitting parameters (φ, δt) measured from densely distributed regional seismic networks operated by China Earthquake Administration (CEA). These stations cover a wide range of geological terranes: from the east part of Central Asian Orogenic Belt, Songliao basin, to the northeast edge of the North China Craton, thus providing us an unprecedented opportunity to image the anisotropic structure and the associated mantle flow beneath northeast China. The image may also help examining various hypotheses and providing constrains in reconstructing the evolution of studied area.

2. Geological Setting

[7] Northeast China is located partly on the North China Craton (NCC) and partly on a portion of the Inner Mongolia-Xing'an fold belt. The NCC, the Chinese part of Sino-Korean Craton, consists of three major blocks: the Eastern, Western Blocks, and the Central Orogenic Belt [*Kusky et al.*, 2007]. As indicated by diamondiferous kimberlites, the NCC remained tectonically stable from its final amalgamation in the early Proterozoic (~1.85 Ga) to the end of the Paleozoic. Thickness of the lithosphere is around 200 km, a typical value observed for a stable Archean craton [*Boyd*, 1989]. However, xenoliths carried up by Cenozoic volcanic extrusions and geophysical images indicate that the lithosphere is no more than 80 km thick over most part of the eastern NCC, which implies that at least 120 km thickness of lithosphere has been removed from the Ordovician to the Cenozoic [e.g., *Menzies et al.*, 1993; *Griffin et al.*, 1998; *Gao et al.*, 2002]. The removal of the keel from a typical Archean craton makes NCC one of the most unique cratons in the world. The dominating mechanism, temporal and spatial evolution of the NCC has been a subject of debate over several decades.

[8] The Inner Mongolia-Xing'an region is a composite fold belt formed by amalgamation of several microcontinental blocks during subduction and collision between the Siberian Craton to the north and the Sino-Korean Craton to the south. During the Paleozoic, three blocks: the Xing'an block to the northwest, the Jimusi massif to the northeast and Songliao block in the central, amalgamated sequentially and formed the collage [*Wu et al.*, 2001]. The Inner Mongolia-Xing'an fold belt is constructed primarily of granites with relatively young ages ~0.5–1.0 Ga, which is approximately the same as the underlying subcontinental lithospheric mantle [*Wu et al.*, 2001]. The Songliao block is mainly composed of the Mesozoic Songliao basin, which is one of the largest oil and gas bearing basins in China with a ~4.3 km sediment thickness in the central. Core samples from continental drilling projects indicate that the basement of Songliao basin is mainly composed of granites, gneiss and Paleozoic strata, some of which have undergone weak metamorphism and deformation.

[9] Multistages of rifting occurred in northeast China beginning from the late Mesozoic [*Ren et al.*, 2002]. Along the Daxing'anling tectonic belt, volcanic activity developed along the NNE or NE directions, indicating a continental extension setting. Development of widespread Basin and Range type fault basin systems represents the second episode rifting, which is characterized by NE–NNE trending half grabens or grabens. The Tancheng-Lujiang (Tanlu) fault, a major lithosphere discontinuity along the eastern Asia, extends to the northeast China along the Jiayi and Dunmi faults (F1 and F2 in Figure 1).

[10] The second major geologic and geophysical feature is the NNE-trending North South Gravity Lineament (NSGL), which roughly runs along the boundary between the Xing'an block and the Songliao basin. This ~100 km wide lineament separates the two regions with very different topographical, tectonic and seismic features [*Xu*, 2007]. The west of the NSGL is characterized by plateaus and highlands with elevations of ~500–3500 m above the sea level, while the east side has an altitude <200 m. Bouguer gravity anomalies increase rapidly from −100 mGal in the west to −40 mGal in the east [*Ma*, 1989]. In contrast to the west side, the east side of the NSGL is characterized by thin crust and lithosphere as well as high heat flow. The importance of the NSGL in the evolution of eastern Asian has been recognized for a long time, however, it is still unclear when and how this lineament formed, and whether it is related to the lithospheric thinning of the NCC.

3. Method of Measurement

[11] We applied an SNR-based multievent approach to obtain the estimate of splitting parameters at a given station. The multievent approach can effectively average splitting variation from different back azimuths, and provide a better parameter estimate for a single-layer HTI (horizontal transverse isotropy) model. The best splitting parameters (φ, δt) were estimated by minimizing either the summed energy in the transverse component

$$E_T(\varphi, \delta t) = \left(\sum_{i=1}^{N} w_i E_{Ti}(\varphi, \delta t) \right) / \sum_{i=1}^{N} w_i, \tag{1}$$

or the summed normalized second eigenvalue λ_2 of the covariance matrix of the corrected particle motion

$$\Lambda_2(\varphi, \delta t) = \left(\sum_{i=1}^{N} w_i \lambda_{2i}(\varphi, \delta t) \right) / \sum_{i=1}^{N} w_i. \tag{2}$$

Here $E_{Ti}(\varphi, \delta t)$ and $\lambda_{2i}(\varphi, \delta t)$ are the transverse energy, and the smaller eigenvalue of the covariance matrix, respectively, after a correction for anisotropy with fast direction φ and delay time δt being made for the ith event. The weight,

w_i, is taken as the averaged SNR of the two horizontal components. The noise time window is chosen right before the SKS time window with the same length as the SKS signal. We also used the total SKS energy recorded at the two horizontal components to normalize the traces before computing the individual $E_{Ti}(\varphi, \delta t)$. In searching the minimum, we chose increments of 1° and 0.05 s for φ and δt, respectively. With the measured (φ, δt), we further calculated the polarization directions of each SKS signal to make sure that they agree with the back azimuths computed from the source-receiver geometry.

[12] On the basis of *Jenkins and Watts* [1968], *Silver and Chan* [1991] proposed to use the following confidence region

$$\frac{E_T(\varphi, \delta t)}{E_T^{\min}} \leq 1 + \frac{k}{n-k} f_{k,n-k}(1-\alpha) \tag{3}$$

to estimate the errors in (φ, δt). Here n is the number of degrees of freedom, α is the confidence level, $k = 2$ is the number of parameters, and f represents the F distribution. Uncertainties estimated from equation (3) are not subjected to the noise level in the data. For noisy data, they could be significant lower than the true level, as any (φ, δt) with $E_T(\varphi, \delta t)$ below the noise level should be considered as a possible solution of the splitting parameters. So we replaced $E_T^{\min}$ in (3) with E^{noise} in calculating the errors in (φ, δt)

$$\frac{E_T(\varphi, \delta t)}{E^{noise}} \leq 1 + \frac{k}{n-k} f_{k,n-k}(1-\alpha), \tag{3'}$$

where E^{noise} is the average of the noise level recorded in the two horizontal components prior to the SKS wave.

4. Data Analysis

4.1. Regional Seismic Stations

[13] We used a total of 129 permanent regional broadband stations, which are mainly composed of Heilongjiang (HL), Liaoning (LN), Jilin (JL), Inner Mongolia (NM), Hebei (HE), and Beijing (BJ/BU) networks (see Figure A1). The regional seismic network was built by a national project that aimed to upgrade and expand the digital seismic network (CSN) in China. Construction was completed in early 2007 [*Zheng et al.*, 2010]. The seismometers are a combination of STS2, GURALP3T, GURALP3ESP, KS2000 and Chinese national broadband sensors JCZ-1 (360 s, 50 Hz), CTS-1 (120 s, 50 Hz), FBS-3 (20 s, 20 Hz) and some other types of sensors. Five stations, DL2, CN2, HEH, HLR and SNY belong to the national network and have been operational since 2001, and another three stations, MDJ, BJT and HIA are GSN stations. Since these stations are relatively well calibrated and have a longer history of recording, we used them to calibrate the sensor orientation for the regional stations.

[14] The 137 stations form a dense 2-D seismic array covering an area of 20° × 15°. The dense 2-D array is ideal for investigating lateral variations in seismic anisotropy. Station spacing varies drastically from region to region, with the highest density of ~20 km in the Yanshan Mountains and over 100 km in the Xing'an ranges. There is no single seismic station in the middle of the Songliao basin, making it difficult to map the deep dynamic structure beneath it.

4.2. Data Selection and Preprocessing

[15] The passive seismic data collected from the regional seismic networks covers a 1 year beginning in July 2007. Teleseismic events with magnitude greater than 5.8 were inspected visually; only events with clear SKS phases were retained. From a total of 27 events, we chose 18 earthquakes with high SNR. In general, we selected data recorded in the epicentral distance range of 85–120°. We also included some records within 83–85° for deep focus (>500 km) earthquakes, provided that the SKS phase is clearly separated from the following S wave in the records. For the eight national/GSN stations, we selected 23 events that occurred between 1 January 2005 and 31 December 2008. Figure 2 shows the distribution of the selected events, with red circles and green diamonds indicating events recorded by regional and national stations, respectively. The events cover three different back azimuths. Most of them are located in the southwest Pacific regions and have back azimuths ranging between 120° and 150°.

[16] Data were recorded continuously at a rate of 100 or 50 samples per second. We resampled the raw data to 20 samples per second, and applied a Butterworth band-pass filter between 1 and 20 s to eliminate low-frequency noise.

4.3. Orientation Corrections for Seismic Stations

[17] Given the very recent completion of the regional seismic networks, calibration of sensor orientation is of great importance. We analyzed the particle motions of teleseismic P waves to determine the azimuth of two horizontal components. This proved to be critical in obtaining the correct estimation of splitting parameters. We followed the same steps as *Niu et al.* [2007] in their estimate of sensor orientation of OBS stations. Assuming that the "north" and "east" components are oriented θ_1 and θ_2 clockwise from the geographic north direction and recognizing that $\theta_2 = \theta_1 + 90°$, we first projected them into the true north and east directions. We further rotated them into the radial and transverse direction based on the given source-receiver geometry. We then computed the weighted summation of the transverse P wave energy for all events. The weight was calculated from the product of SNR and linearity of the P wave particle motion. Finally, we chose θ_1 as the orientation of the "north" component when the summed P wave energy in the transverse component reaches its minimum.

[18] The total number of events used for orientation estimates for each station ranges between 13 and 50, and for 90 percent of the stations, the number is greater than 20. We noticed that for the five national stations SNY, DL2, CN2, HEH and HLR, which began to operate in 2001, the estimated orientations of the north component are within ±9° with a small standard deviation. Thirty percent of the newly installed stations are misoriented by >20°, with some up to ~90° and 180°. Stations with $\theta_1 > 10°$ are listed in Table 1. We also used the P wave particle-motion analysis to confirm the consistency in instrumentation at each station during the 1 year period. The correction of instrumental orientation is critical to obtain correct splitting parameters, which was also addressed for a GSN station (ULN) in the work of *Liu et al.* [2008]. Details about estimation of sensor orientation of the Chinese Regional Seismic Networks can be found in the work of *Niu and Li* [2010].

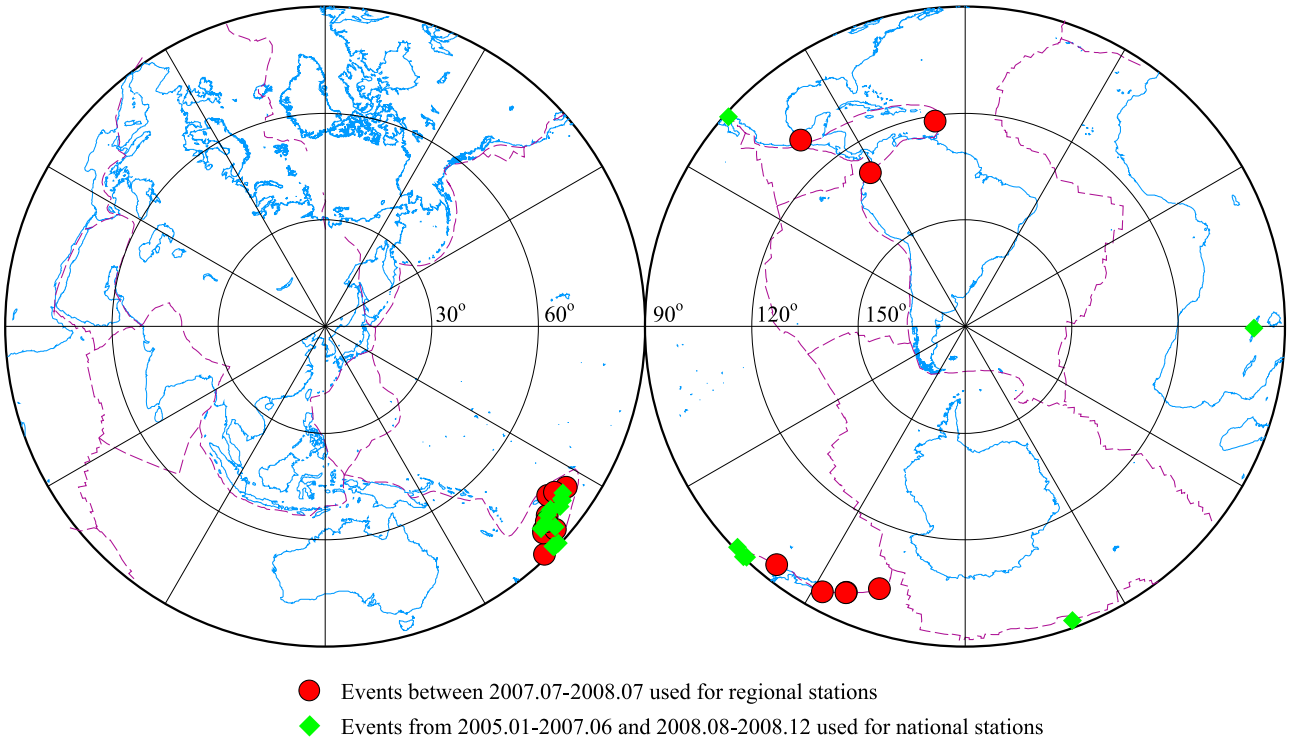

Figure 2. Locations of the events used in this study. Red circles and green diamonds indicate events recorded by the regional and national stations, respectively. Azimuthal equidistant projection centered on 126°E and 43°N is used.

4.4. SKS Splitting Measurements

[19] Figure 3a shows the radial and transverse component of the waveform data recorded by the LN regional network from a deep event occurring at the Tonga subduction zone. The SKS signal shown in the transverse component at most stations appears to be much stronger than the noise. Besides the large amplitude observed in the transverse component, the SKS phase also exhibits an elliptical particle motion. Both indicate the existence of seismic anisotropy beneath these stations. In Figure 3b, we show the transverse components after being corrected with splitting parameters obtained from the two different methods. Obviously, energy within the SKS arrival time window is reduced to the noise level.

[20] Figure 4 shows an example of the SKS waveforms recorded at station HL.JIY. The original 3 components are shown in Figure 4a, the transverse and radial components after correcting seismic anisotropy are shown in Figure 4b, and particle motions of the SKS wave before and after the correction are shown in Figures 4c and 4d. The color contour map of the weighted summation of the transverse energy E_T and the smaller eigenvalue Λ_2 in the (φ, δt) space is shown in Figures 5a and 5b, respectively. For almost all the splitting measurements, the values of φ and δt determined from the method are virtually identical to each other (Table 2).

[21] We regarded the measured splitting parameters as reliable only when they satisfy the following criteria: (1) energy on the transverse component is significantly reduced after the correction of anisotropy, (2) difference in the fast-axis direction measured from the two methods is small (within the error), and (3) the measurements are not

Table 1. BHN Azimuth[a]

Station	Number of Events	BHN Orientation (deg)
BJ.NKY	42	−14 ± 3
BJ.XBZ	18	−13 ± 4
BU.MDY	24	15 ± 3
BU.TST	32	176 ± 4
BU.ZHL	35	95 ± 3
HE.WEC	38	−18 ± 3
HL.BEL	28	−16 ± 3
HL.FUY	18	179 ± 5
HL.JMS	38	152 ± 4
HL.MOH	41	−11 ± 3
HL.QAN	28	27 ± 3
HL.QTH	18	−10 ± 2
HL.XBH	18	−27 ± 4
JL.BCT	43	112 ± 2
JL.CBT	26	−95 ± 3
JL.DHT	40	180 ± 3
JL.JCT	30	111 ± 3
JL.LHT	29	180 ± 3
JL.MJT	37	−55 ± 4
JL.PST	41	−155 ± 3
JL.SPT	43	−97 ± 3
JL.SYZT	40	−89 ± 4
LN.ANS	45	17 ± 3
LN.FSH	43	−18 ± 3
LN.HUR	44	13 ± 3
LN.LYA	47	15 ± 3
NM.CHR	25	11 ± 3
NM.GNHH	41	−96 ± 2
NM.IDR	21	−13 ± 2
NM.ZLT	34	−11 ± 4

[a]Only stations with azimuth >10° are listed.

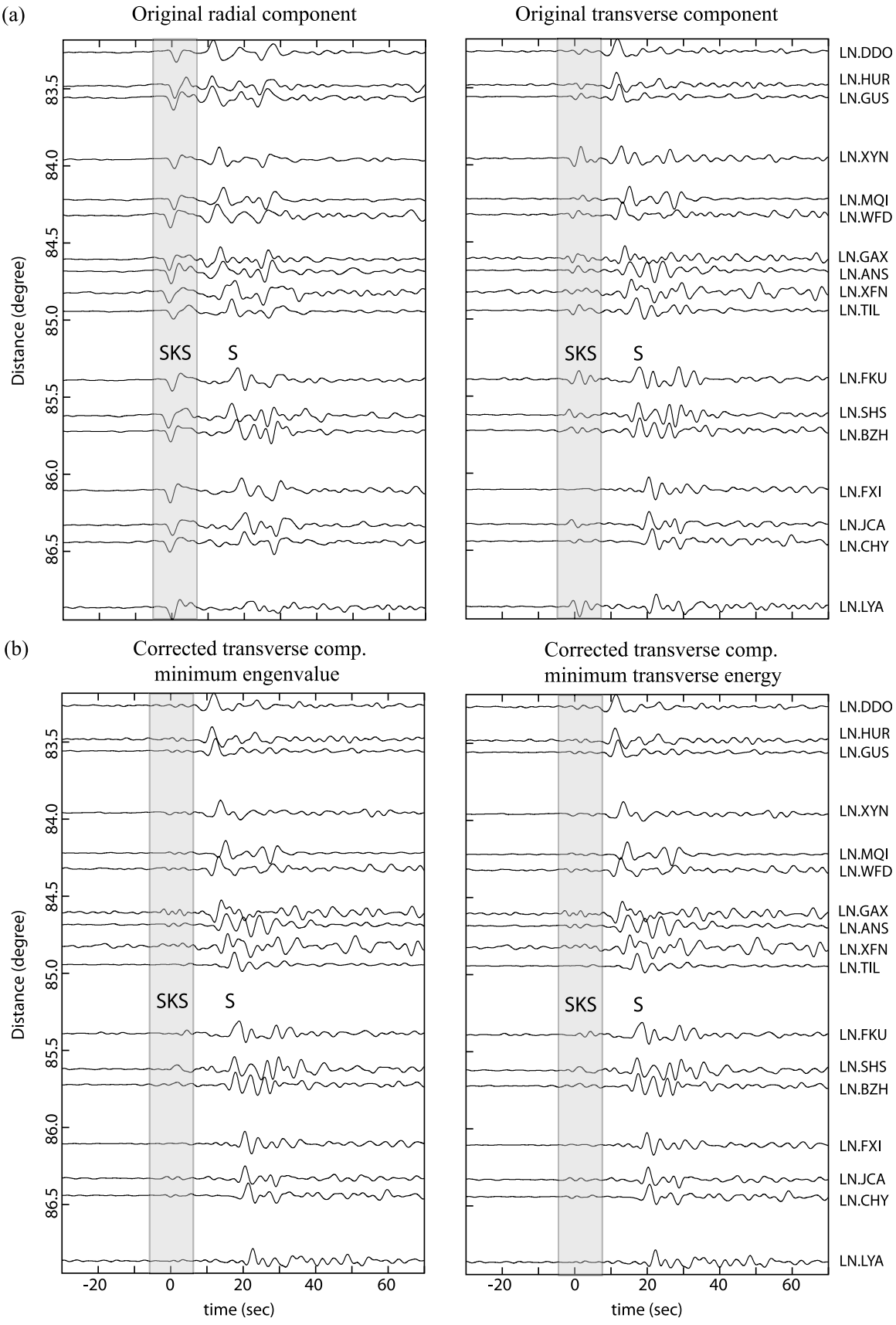

Figure 3. (a) Radial and transverse component of the seismograms recorded by the Liaoning (LN) regional network from a deep event occurring in the Tonga subduction zone. (b) Transverse components after being corrected by the measured seismic anisotropy.

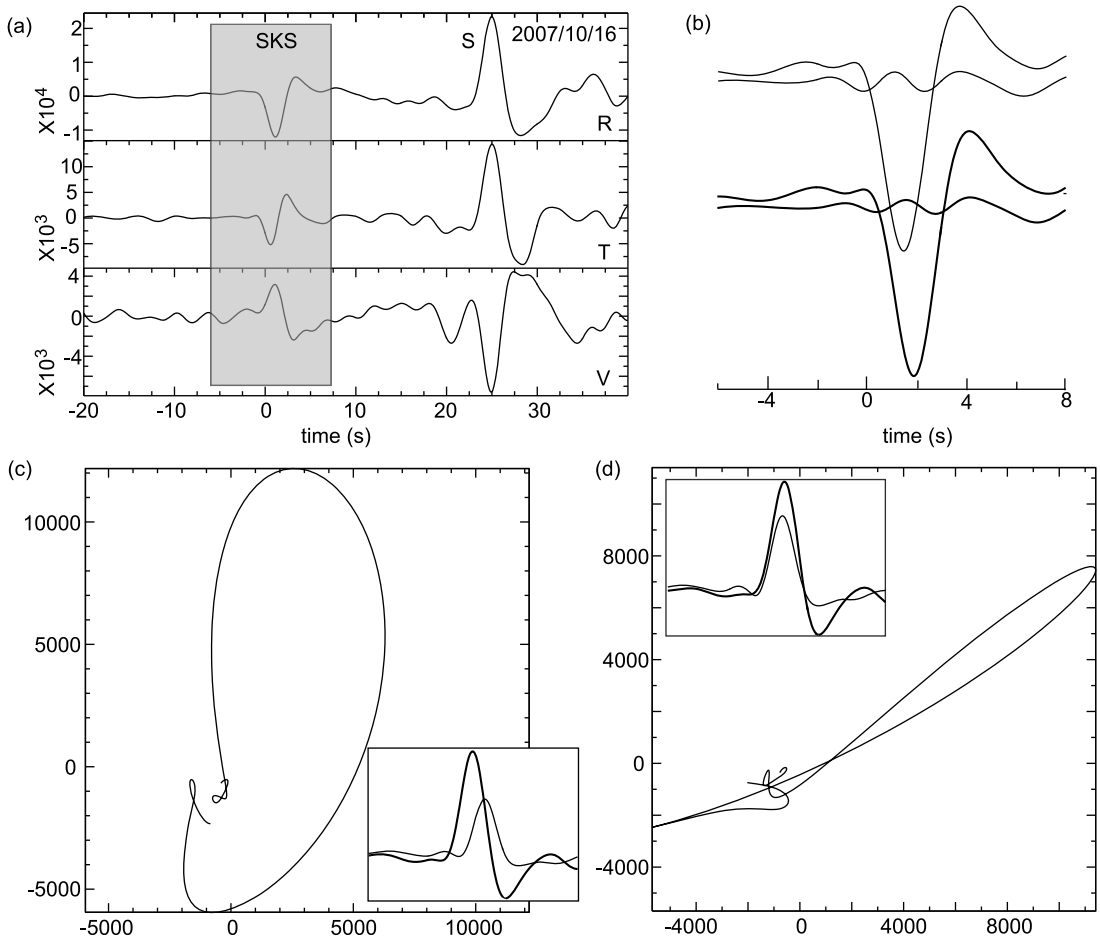

Figure 4. An example of estimating splitting parameters at station HL.JIY. (a) The original three components. (b) Transverse and radial components corrected with the anisotropic parameters determined from the first (thin lines) and the second (thick lines) methods. (c and d) Particle motions before and after the splitting correction, respectively. Insets show the fast and slow components of the SKS wave before (Figure 4c) and after (Figure 4d) the splitting correction.

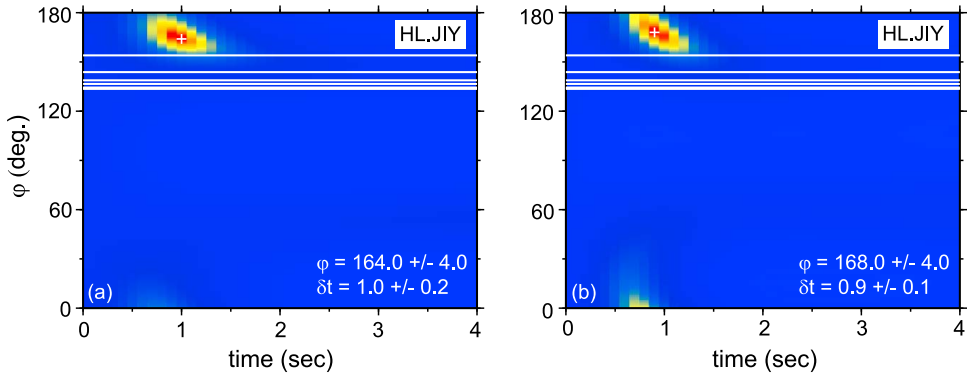

Figure 5. (a) Weighted summation of the transverse energy E_T and (b) the smaller eigenvalue Λ_2 are shown as a function of the assumed splitting time, δt, and fast-axis direction, φ. Seven events were stacked to obtain the splitting parameters. The white plus indicates their minimums in the (φ, δt) space. White lines show the back azimuths directions of the incoming SKS waves used in the measurement.

Table 2. SKS Splitting Parameters for Stations Beneath Northeast China

Station	Number of Events[a]	Number of Azimuth[b]	Minimizing Transverse Energy[c]				Minimizing Eigenvalue[d]				Type[e]
			Φ (deg)	ΔΦ (deg)	δt (s)	Δδt (s)	Φ (deg)	ΔΦ (deg)	δt (s)	Δδt (s)	
Southeast of Songliao Basin (Region A)											
LN.ANS	6	1	134	4	1.3	0.3	134	4	1.2	0.2	
LN.BEP	7	1	129	2	1.8	0.6	132	3	1.5	0.7	Nodal
LN.BXI	5	1	148	8	0.4	0.2	143	5	0.5	0.2	Nodal
LN.BZH	10	1	117	6	0.6	0.2	115	6	0.5	0.2	
LN.CHY	7	1	132	3	1.6	0.5	132	3	1.7	0.3	Nodal
LN.DDO	7	1	135	4	0.9	0.4	139	3	0.9	0.3	
LN.FKU	7	1	177	11	0.5	0.2	171	14	0.6	0.1	
LN.FSH	5	1	152	5	0.7	0.2	146	4	0.9	0.2	
LN.FXI	8	1	135	3	1.1	0.3	134	3	1.1	0.3	Nodal
LN.GAX	6	1	135	2	1.8	0.5	135	2	1.9	0.3	Nodal
LN.GUS	6	1	146	5	0.8	0.3	148	5	0.8	0.2	Nodal
LN.HSH	7	1	110	6	0.6	0.2	115	4	0.7	0.1	
LN.HUR	7	1	127	5	0.6	0.2	130	3	0.7	0.2	
LN.HXQ	6	1	143	4	1.0	0.4	147	4	0.9	0.2	
LN.JZH	7	1	47	3	1.1	0.5	133	3	1.1	0.3	Nodal
LN.KDN	4	1	120	11	0.7	0.2	123	7	0.8	0.2	
LN.LHT	6	1	148	3	0.9	0.2	144	3	1.1	0.2	
LN.LYN	5	1	132	4	0.7	0.4	134	3	0.8	0.3	
LN.MQI	7	1	137	3	1.4	0.4	132	3	1.4	0.2	
LN.QYU	3	1	152	4	1.0	0.2	157	4	0.9	0.1	
LN.TIL	6	1	177	9	0.6	0.2	173	9	0.7	0.2	
LN.WFD	7	1	136	4	1.1	0.4	138	4	1.2	0.3	
LN.XFN	5	1	137	6	0.9	0.4	141	5	0.8	0.4	Nodal
LN.XYN	7	1	161	8	0.7	0.2	155	6	0.8	0.2	
JL.CBT	4	2	136	11	0.4	0.3	137	12	0.4	0.3	Null
JL.DHT	6	1	144	5	0.8	0.3	143	4	0.9	0.3	
JL.FMT	5	1	152	8	0.5	0.2	160	10	0.4	0.1	Null
JL.FST	6	2	129	22	0.2	0.4	139	8	0.3	0.4	Null
JL.JCT	4	1	108	6	0.7	0.2	109	6	0.7	0.2	
JL.LHT	7	1	130	5	1.0	0.3	129	4	1.0	0.3	
JL.MJT	6	1	13	22	0.2	0.2	142	12	0.3	0.2	Null
JL.PST	7	1	139	4	1.2	0.4	132	4	1.3	0.2	
JL.SPT	5	1	114	3	0.9	0.2	113	3	0.9	0.1	
JL.SYZT	8	2	164	16	0.5	0.2	157	13	0.5	0.2	
JL.THT	5	1	131	6	0.8	0.3	128	7	0.6	0.2	
JL.YNB	5	1	160	9	0.7	0.3	150	5	0.9	0.2	
CB.CN2	9	2	147	6	0.7	0.2	151	7	0.6	0.2	
CB.SNY	7	1	146	4	1.1	0.3	148	4	1.0	0.2	
CB.DL2	9	2	113	6	0.6	0.2	122	4	0.8	0.2	
HL.XBH	4	1	78	10	0.6	0.2	80	13	0.6	0.2	
IC.MDJ	9	2	97	8	0.7	0.2	98	11	0.7	0.2	
Jiamusi Massif (Region B)											
HL.BAQ	5	1	161	3	1.7	0.2	162	3	1.7	0.2	
HL.FUY	3	1	172	4	1.1	0.2	169	4	1.2	0.1	
HL.JIY	7	1	164	4	1.0	0.2	168	4	0.9	0.1	
HL.JMS	6	1	147	3	1.4	0.3	146	2	1.5	0.2	
HL.LBE	6	2	153	4	1.2	0.3	156	5	1.1	0.3	
HL.MIH	4	1	151	4	1.1	0.3	150	4	1.1	0.2	
HL.QTH	3	1	154	4	0.7	0.2	153	3	0.7	0.1	
HL.SYS	6	2	148	5	0.7	0.3	146	4	1.0	0.2	
HL.XUK	5	2	172	5	1.2	0.3	176	5	1.2	0.2	
Daxing'anling (Region C)											
HL.JGD	11	1	138	3	1.0	0.3	138	2	1.0	0.2	
HL.MOH	7	1	10	10	0.3	0.1	14	6	0.3	0.1	Null
NM.ARS	7	2	154	9	0.5	0.1	154	7	0.5	0.1	
NM.CHR	4	2	173	11	0.5	0.2	174	9	0.5	0.2	
NM.GNHH	9	2	119	4	0.6	0.2	124	3	0.8	0.2	Nodal
NM.IDR	5	1	156	4	1.0	0.2	158	4	1.0	0.2	
NM.JIP	8	1	114	3	1.1	0.3	110	3	0.9	0.2	
NM.MZL	7	1	147	4	0.8	0.2	147	4	0.8	0.2	
NM.ZLT	11	2	157	6	0.8	0.2	167	12	0.7	0.2	
IC.HIA	25	3	154	5	0.8	0.2	152	5	0.8	0.1	
CB.XLT	15	2	106	5	0.5	0.2	105	5	0.5	0.1	
Yanshan Mountains (Region D)											
BJ.BBS	8	1	81	8	0.8	0.2	86	9	0.8	0.1	
BJ.DHC	7	1	83	6	0.7	0.1	83	7	0.7	0.2	
BJ.LBP	6	1	84	7	0.8	0.2	84	9	0.8	0.2	
BJ.LLM	3	2	62	5	0.7	0.2	68	6	0.7	0.1	

Table 2. (continued)

Station	Number of Events[a]	Number of Azimuth[b]	Minimizing Transverse Energy[c]				Minimizing Eigenvalue[d]				Type[e]
			Φ (deg)	ΔΦ (deg)	δt (s)	Δδt (s)	Φ (deg)	ΔΦ (deg)	δt (s)	Δδt (s)	
BJ.MIY	11	1	76	6	0.8	0.1	76	7	0.8	0.1	
BJ.NKY	7	1	105	4	0.7	0.2	104	4	0.7	0.1	
BJ.SSL	9	1	94	5	0.8	0.1	92	6	0.8	0.2	
BJ.XBZ	5	1	90	4	0.7	0.1	90	4	0.7	0.1	
BJ.ZHT	7	1	70	10	0.5	0.1	69	10	0.5	0.1	
BU.BDH	8	1	135	3	1.6	0.5	136	3	1.6	0.4	Nodal
BU.GUY	4	1	104	4	1.6	0.2	110	5	1.7	0.2	
BU.LQS	7	1	102	5	0.9	0.2	100	7	0.8	0.2	
BU.MDY	9	1	93	7	0.9	0.2	93	8	0.9	0.2	
BU.SFS	9	2	101	10	0.5	0.2	102	9	0.5	0.2	
BU.SHC	4	1	71	6	0.7	0.1	76	5	0.6	0.2	
BU.SZL	5	1	66	5	1.0	0.2	73	5	0.9	0.2	
BU.TST	10	2	77	20	0.4	0.2	91	22	0.5	0.2	
BU.XUH	9	1	83	14	0.5	0.2	85	19	0.5	0.2	
BU.ZHL	8	1	87	16	0.5	0.2	91	17	0.5	0.2	
BU.ZUH	6	1	108	5	0.7	0.2	106	3	0.7	0.1	
HE.CHC	6	1	99	3	1.0	0.1	100	3	1.0	0.1	
HE.CLI	8	1	131	2	1.1	0.3	131	2	1.1	0.2	Nodal
HE.FEN	5	1	100	4	1.0	0.2	99	4	1.0	0.1	
HE.KUC	4	1	102	3	1.3	0.2	103	4	1.3	0.1	
HE.QIL	4	1	96	8	0.7	0.2	99	7	0.7	0.2	
HE.WEC	8	1	134	3	1.0	0.3	131	3	1.1	0.2	Nodal
HE.XIL	3	1	55	3	1.1	0.2	57	3	1.0	0.2	
HE.XLD	4	1	49	3	0.9	0.3	128	3	0.8	0.2	Nodal
IC.BJT	18	1	95	8	0.5	0.1	94	9	0.5	0.1	
LN.JCA	10	1	89	11	0.5	0.2	88	12	0.5	0.2	
LN.LYA	10	2	92	5	0.8	0.2	91	5	0.8	0.1	
LN.SHS	5	1	93	9	0.6	0.2	86	10	0.6	0.1	
NM.BAC	10	1	107	3	1.1	0.2	108	3	1.1	0.2	
Other Regions (Around Songliao Basin or Across the NSGL)											
HL.BEL	5	1	142	2	1.7	0.3	143	3	1.6	0.3	Nodal
HL.QAN	4	2	45	3	2.2	1.8	136	4	1.0	0.5	Nodal
HL.TOH	7	1	141	5	0.5	0.4	144	5	0.4	0.3	Null
HL.YAS	7	2	132	7	0.6	0.5	129	7	0.3	0.2	Null
HL.YIL	4	1	158	4	0.5	0.1	167	6	0.4	0.1	Null
HL.NEH	5	1	25	4	0.7	0.2	24	4	0.7	0.2	
HL.NZN	10	1	149	4	0.8	0.2	150	4	0.8	0.1	
HL.TAH	7	2	36	3	0.6	0.2	38	3	0.6	0.2	
JL.BCT	10	1	75	7	0.7	0.2	80	9	0.6	0.2	
NM.AGL	5	1	23	6	0.4	0.2	21	5	0.4	0.1	Null
NM.LUB	6	1	60	10	0.4	0.2	62	9	0.4	0.2	Null
NM.NIC	6	1	140	5	0.5	0.2	140	4	0.5	0.2	Nodal
NM.TIS	6	1	20	3	0.8	0.2	21	3	0.8	0.2	
CB.HEH	8	1	36	3	1.1	0.3	35	3	1.2	0.3	Nodal

[a]Number of events used in the shear wave splitting analysis for a certain station.
[b]Number of quadrant of back azimuths of events used in each measurement for a certain station. Generally, the events used mostly come from the South Pacific with a back azimuthal range 120~150°.
[c]Measurements from method of minimizing the transverse energy of the corrected waveform.
[d]Measurements from method of minimizing the smaller eigenvalue λ_2.
[e]Remarks for nodal and null measurements. A nodal measurement means the difference between back azimuth and fast direction is less than 15°, while a null one indicates a weak anisotropy with a delay time being less than 0.4 s.

affected by the selection of time window length. We found that if the instrument is misoriented and is not corrected, the two methods could yield a significant difference in estimating the fast-axis direction. SNR is not listed as a specific criterion, since we already considered it as a weight in the summation for different events in searching the best (φ, δt). When the fast direction φ is nearly parallel or perpendicular to the arriving direction of the SKS wave, energy projected to the slow or fast direction is very limited, resulting in little or no splitting of SKS waveform. In this case, we considered the fast direction to be constrained, which is either parallel or perpendicular to the incoming SKS ray direction. In our study, if the difference between the estimated fast direction and the back azimuths of all the events falls below 15°, we marked this measurement as a "nodal" one. We regarded a measurement as "null" when the splitting time δt is less than 0.4 s even with good azimuthal coverage, which indicates seismic anisotropy is weak or absent beneath the station.

5. SKS Splitting Observations

[22] We obtained a total of 108 splitting measurements with good quality from the six regional seismic networks. Figure 6 shows the 108 measurements, which include 17

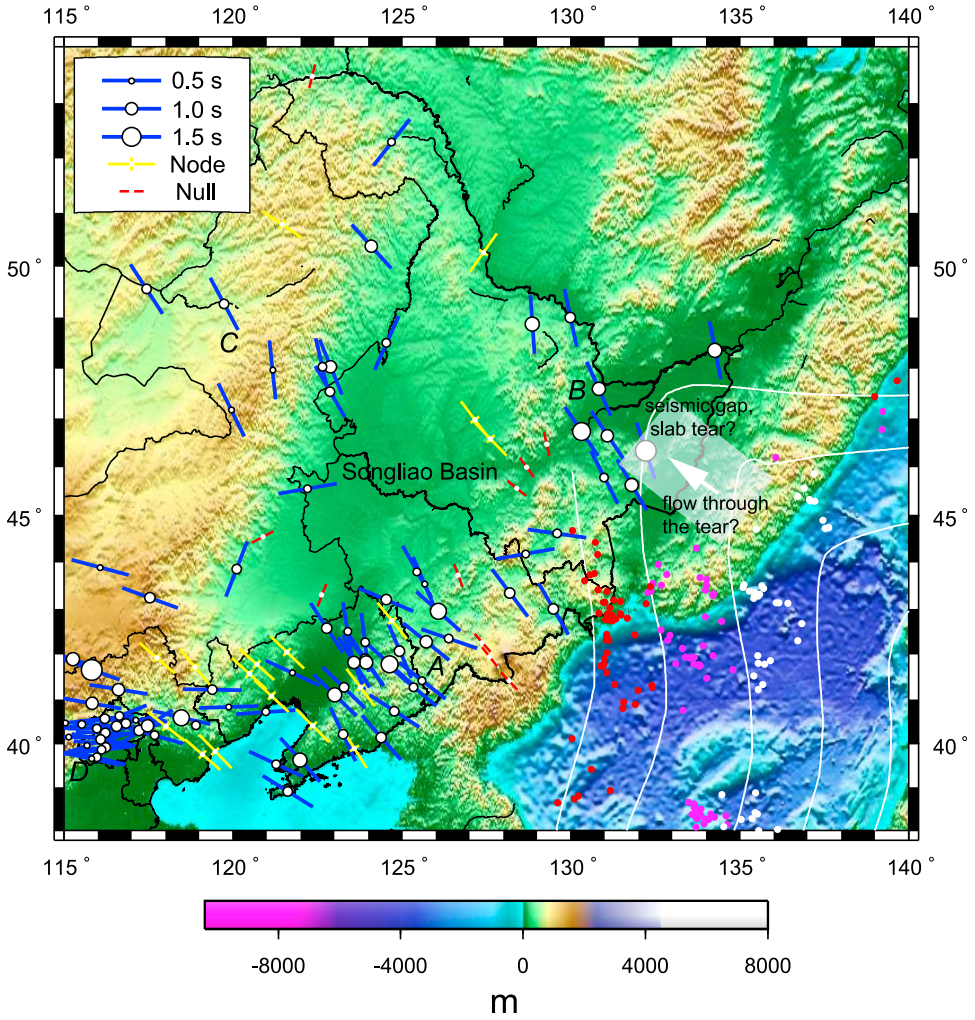

Figure 6. Map showing the measured fast directions and splitting times at the 108 stations. The fast-axis direction is shown by a bar line, and the amount of splitting is indicated by the size of the circle plotted at station locations. Red symbols represent "null" measurements with $\delta t < 0.4$ s, and yellow symbols with long and short crossing legs denote "nodal" measurements, corresponding to a φ either perpendicular or parallel to the back azimuths of the incoming rays. Capital letters A, B, C, and D represent the four subregions discussed in the main text. Deep seismicity is shown as solid dots (white: 300–400 km; purple: 400–500 km; red: >500 km). The shaded area and the white arrow indicate a speculative slab tear and the associated mantle flow.

"nodal" (yellow) and 10 "null" measurements (red). We also listed the two sets of measurements of (φ, δt) in Table 2. The table is organized by grouping stations into the following tectonic regions (Figure 1): the southeast Songliao basin (region A), Jiamusi block (region B), Inner Mongolia-Xing'an fold belt (region C), and Yanshan Mountains (region D).

[23] The ensemble of fast axis directions with the delayed times shown in Figure 6 provides a comprehensive picture of the mantle deformation beneath northeast China. Several distinguishing features can be found from the obtained splitting parameters. Anisotropy beneath the studied region is relatively small with an average splitting time of 0.8 s. Most stations show a NW–SE fast polarization, parallel to the regional extension direction. There are also noticeable changes in the measured fast direction across the region, especially the asymmetrical pattern around the Songliao basin. Starting from the southeast corner of the basin, we saw a "normal" NW–SE fast axis, roughly perpendicular to the Changbaishan mountain range (region A). The NW–SE trend rotates slightly to NNW toward north, where the geometry of the subducting slab changes sharply with an almost 90° turning (region B). To the west of Songliao basin in the Great Xing'an Range, the fast axis direction shows some variations with a reduced splitting time (region C). Within the Yanshan mountain range (region D), the fast axis aligns rather consistently along the EW direction that is parallel to the strike direction. In the following sections, we'll show the observed anisotropic features and related mantle deformation in each subregion sequentially.

5.1. Southeast Corner of the Songliao Basin

[24] A first look at the anisotropy map shown in Figure 6 reveals a dominant NW fast axis direction at the southeast corner of the Songliao basin. This subregion is roughly bounded by the Tanlu fault to the west, Jimusi block to the north, and is located mainly on the Archean North China Craton. The dominant strike direction of major basement faults in this region is NNE. Shear wave splitting is observed at 41 stations, which are mainly from Liaoning and Jilin regional networks. The number of events used for each measurement ranges from 3 to 10. Almost all the incoming rays are from the southwest Pacific region within a narrow back azimuthal range ~N120°E–N150°E. The average fast direction and splitting time is 134° and 0.85 s, corresponding to a layer of 96 km in thickness if an average of 4% anisotropy is assumed [*Silver*, 1996]. It should be noted that there's a tradeoff between the anisotropy strength and the estimated layer thickness.

[25] We have eight "nodal" and four "null" measurements in this region. According to our definition, we named a measurement "nodal" when the difference between the back azimuths of all the events and the measured fast direction is less than 15°. This occurs when the fast direction is either parallel or perpendicular to the polarization direction of the incoming waves. All the events used to obtain the eight "nodal" estimations were at back azimuths of 130° to 150°, consistent with a NW–SE fast direction observed at nearby stations. We noticed that three of the four "null" observations are located around the Changbaishan volcano which is close to the boundary between North Korean and northeast China. Events used for those "null" measurements range from 4 to 6. Teleseismic P tomographic images show a low-velocity anomaly extending to 300 km depth beneath the Changbaishan volcano [e.g., *Huang and Zhao*, 2006]. We suggest that this local-scale asthenospheric injection might be responsible for the null observation.

[26] We observed a NW–SE fast axis direction (122 ± 4°) beneath DL2 (38.90°N, 121.63°E) station, one of the national stations, which is located in the Bohai bay region. The direction we obtained is a little different from the estimate of 95° ± 6° of *Liu et al.* [2008]. Our estimated splitting time δt is ~0.8 ± 0.2 s, smaller than their measurement of 1.5 ± 0.4 s. The difference might be due to the number of events used in the measurements.

5.2. Northeast Corner of the Songliao Basin: The Jiamusi Massif

[27] The Jiamusi massif is located in the eastern part of the Central Asian Orogenic Belt. It consists mainly of two metamorphic assemblages: one is the granulite-facies Mashan Group and the other blueschist-facies Heilongjiang group. The later one is considered as an ophiolitic assemblage that represents a disappeared ocean between the Jiamusi massif and Songliao block [*Wu et al.*, 2001].

[28] An obvious feature can be found from the nine observations located in the Jiamusi block. The fast axis direction rotates clockwise to NNW, and the averaged 1.2 s splitting time is among the largest of the whole studied region. If we assume a layer with the same degree of anisotropy (4%), a 135 km thick layer is then required. The geometry of the subducting west Pacific plate changes sharply beneath the Jimusi block, which might be related to the observed feature, and we will discuss this in section 6.4.

5.3. West Bound of the Songliao Basin: The Inner Mongolia-Xing'an Fold Belt

[29] The Inner Mongolia-Xing'an fold belt is part of the Central Asian Orogenic belt, which lies between the Siberian and Sino-Korean Craton [*Sengör and Natalin*, 1996]. Our observations are mostly from the NNE-striking Great Xing'an Range, which is characterized by huge volumes of Mesozoic volcanic rocks and granites. Multiple episodes of contractional to extensional deformation occurred in this region in Late Mesozoic, presumably as the result of the collision between the amalgamated North China-Mongolia block and the Siberian block. The most prominent geologic and geophysical feature, the ~3500 km long NSGL starts from here. This ~100 km wide lineament zone marks the steepest gravity gradient in China. The surface topography also increases from <200 m in the east to >1500 m in the west [*Xu*, 2007].

[30] We have a total of 11 measurements west of the NSGL, which exhibit large deviations in the fast-axis direction with a reduced amplitude. One of the GSN stations, HIA (49.27°N, 119.74°E), is located on the Hailar basin situated on this Paleozoic orogenic belt. We used a total of 25 events with a wide range of back azimuths (Figure 2) to find the best fitting (φ, δt), which are 152 ± 5° and 0.8 ± 0.1 s, respectively. The fast direction is oblique to the dominant NE–SW strike direction of the region. Many measurements have been made for this station, e.g., by *Liu et al.* [2008], 160 ± 7°, 0.8 ± 0.1 s, and by *Silver and Chan* [1991], 160 ± 5°, 0.7 ± 0.2 s. In general, our observation is very consistent with their results. The same splitting parameters are observed at a nearby station NM.MZL, which is located ~200 km west of HIA.

[31] To the south of Inner Mongolia fold belt, a rotation of the fast-axis orientation from NNE to NEE was observed. The new direction tends to align with the strike of the Yanshan mountain range. The national network station XLT (43.9°N, 116.08°E) is located in the late Paleozoic orogenic belt that runs nearly east west. Fifteen events from two different back azimuths were used to constrain the splitting parameters (105 ± 5°, 0.5 ± 0.1 s). We noticed that our estimation here is very different from previous SKS splitting result of *Liu et al.* [2008] (40 ± 16°, 0.5 ± 0.2 s). One possible reason for this discrepancy is the weak anisotropy observed at this station.

5.4. Southwest Corner of the Songliao Basin: Yanshanian Orogenic Belt

[32] The southwest portion of the studied region is located partly on the Yanshan belt. The Yanshanian orogenic belt is characterized by intensive contractional deformation manifested as folds, recumbent folds, and reverse faults [*Deng et al.*, 2007], marking the reactivation of NCC during the Yanshanian time (Jurassic-Cretaceous). Approaching Yanshan belt from north, we found an anticlockwise rotation in the fast-axis direction, from NWW to almost E–W, nicely aligning with the strike of the belt. We have a total of 33 measurements in this area. Most stations showed a

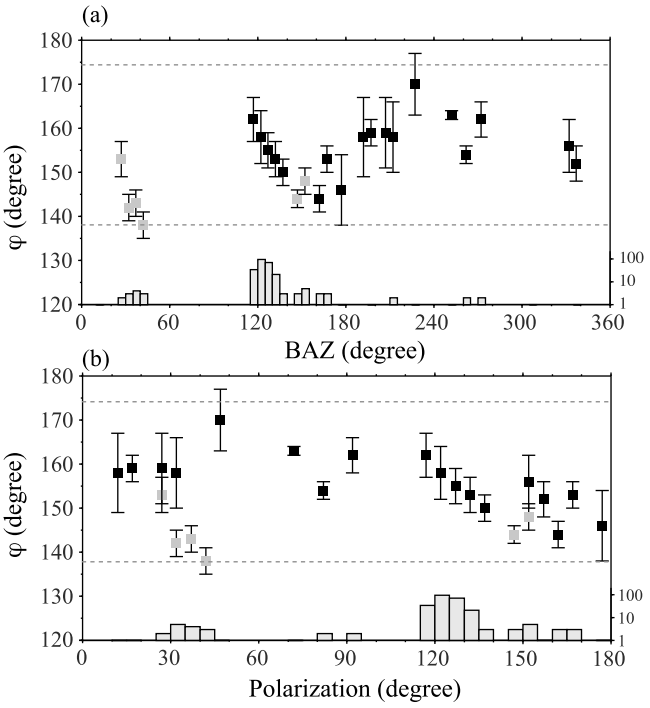

Figure 7. Apparent fast-polarization directions estimated from the 24 five degree bins is shown as a function of (a) the back azimuth and (b) the polarization direction of the incoming SKS wave. Black and gray squares indicate regular and "nodal" measurements, respectively. Variations in the apparent fast direction are <±10%, which are indicated by the two dashed lines. The number of events used in each bin is shown in the lower part of the plot. Note that no obvious $\pi/2$ periodicity is shown in the data.

consistent fast direction close to EW. Splitting times vary from 0.5 s to 1.3 s with an average value of ~0.8 s. This would require an accumulation of splitting for an S wave traveling through a ~90 km thick layer with 4% anisotropy.

[33] The BJT station (40.02°N, 116.17°E) is located at the boundary of the Yanshanian fold belt and the Huabei plain. The splitting parameters measured from 18 events is 94 ± 4°, 0.5 ± 0.1 s. Numerous measurements have been made for this station. For example, *Liu et al.* [2008] obtained 112 ± 10°, 0.8 ± 0.3 s for φ and δt, respectively, from 35 events, which seems to be consistent with our result. Meanwhile, *Zhao et al.* [2007b] reported a mean φ of 59 ± 5°, which appears to be inconsistent with the measurements from the nearby stations.

6. Discussion

[34] For all the stations, we measured (φ, δt) with the two method described in section 3. Among the 108 stations, 104 showed almost similar results between the two methods. The estimated fast directions from the two methods are perpendicular to each other for three other "nodal" stations (LN.JZH, HE.XLD, and HL.QAN), which reflect the intrinsic ambiguity of the "nodal" measurement. For one "null" station (JL.MJT) the fast directions determined from the two methods are 13° ± 22° and 142° ± 12°, respectively. The measured splitting times from the two methods are, however, consistent with each other. Thus the two methods gave consistent estimates of seismic anisotropy for all the 108 stations. As the projection of SKS wave energy to the transverse component can be affected by misorientation of instruments or deviations from 1D raypath induced by a dipping structure, measurements from the first method that minimizes the SKS energy in the transverse component could be biased by these effects. Therefore, we selected the measurements from the second method as our final results.

[35] The depth resolution of the nearly vertical SKS wave is known to be low. The anisotropic region(s) can be anywhere along the *S* wave raypath in the receiver side. Although anisotropy within the crust beneath the station could contribute partly to the observed SKS splitting, many studies [e.g., *Silver*, 1996] found the averaged splitting time caused by crustal anisotropy to be around 0.2 s. *Iidaka and Niu* [2001] measured the crustal anisotropy with the Moho reverberation phase PpSms and found that the splitting time is <0.1 s beneath the GSN station, MDJ, which is located in our study area. *Wu et al.* [2007] analyzed the local S waves and found that the crust-induced splitting times are between 0.1 and 0.3 s beneath north China. We thus assume that the main source of the observed anisotropy is located in the upper mantle.

[36] We have assumed a single homogeneous anisotropic layer with a horizontal symmetry axis to explain the observed SKS waveform data with the multievent stacking analysis. Under this assumption, φ and δt measured from SKS waves arriving from different back azimuths is expected to have the same values. This assumption, however, is violated in the presence of more complicated anisotropic structure. The complexity can arise from a dipping symmetry axis and depth variation in anisotropy and has been found in many continental regions [e.g., *Savage and Silver*, 1993; *Silver and Savage*, 1994; *Schulte-Pelkum and Blackman*, 2003; *Tian et al.*, 2008]. In these cases, φ and δt are no longer independent of the polarization direction of the incoming wave. One can use this relationship to investigate the nature of the anisotropy beneath a station provided that an SKS data set with good back azimuthal coverage is available.

[37] As the CDSN HIA station has the longest recording time in our study area, we chose it to investigate back azimuthal variations in splitting parameters. We selected a total of 324 earthquakes occurring between 1990 and 2008 with SNR of SKS in the radial component greater than 2. We sorted them according to their back azimuth and further grouped them into 5° bins. We obtained 18 regular and 6 nodal measurements of φ, which are shown as black and gray squares in Figure 7. The 24 back azimuths cover all of the four quadrants and the estimated φ varies within the azimuthal range of 138–170°, with an average of 153° and a standard deviation of 6° (Figure 7a). *Rumpker and Silver* [1998] computed the apparent splitting parameters for models with multiple anisotropic layers. For models with relatively small variations of anisotropy with depth, the calculated apparent fast direction φ_a changes <10% over most of the back azimuthal range, and φ_a reflects the averaged fast direction of the anisotropic layers. It also seems that the characteristic $\pi/2$ periodicity of a two-layer anisotropic medium is not clearly shown here (Figure 7b). We

thus regard the one-layer model as a good approximation of the anisotropic structure beneath HIA, and conclude that the multievent method is a proper way to obtain robust estimates of splitting parameters.

[38] The SKS waves recorded at most of the stations come from a narrow range of directions, making it impossible to conduct the same type of analysis. In this case it is reasonable to assume that φ and δt estimated from individual events are the same, and the multievent measurement is expected to be more reliable because of the improved SNR. For stations with more than one back azimuth, we manually checked the consistency between different events as well as the agreement with the adjacent stations.

[39] Generally, two competing hypotheses are always proposed to account for the observed seismic anisotropy in continental settings. One hypothesis is that seismic anisotropy lies in the sublithospheric mantle associated with asthenosphere flow [*Silver*, 1996; *Savage*, 1999; *Fouch and Rondenay*, 2006]. The other hypothesis is that the observed anisotropic structure reflects a vertically coherent deformation in the lithosphere [*Silver*, 1996]. Here, we examine four different flow models that may contribute to the observed complexity in the study area: (1) asthenospheric flow related to present-day absolute plate motion, (2) "frozen" mantle deformation associated with the regional extension occurring in late Mesozoic and Cenozoic time, (3) small-scale mantle flow associated with edge-driven convection, and (4) mantle flow associated with the eastward retreat of the subduction.

6.1. Relationship With a Simple Asthenosphere Flow

[40] The first hypothetic model that we would like to examine here is whether the observed seismic anisotropy is dominated by a large-scale asthenospheric flow associated with absolute plate motion (APM). On the basis of the HS3-NUVEL-1A model [*Gripp and Gordon*, 2002], the APM for our studied region is N64°W (location: 45°N, 130°E) with a velocity of 2.0 cm/a. Although many stations show a fast-axis direction more or less parallel to the AMP, it is very clear that this mechanism alone cannot explain all the observations. We found noticeable variations in fast-axis direction as well as in splitting time that exist in both regional (<1000 km) and local (<200 km) length scales, suggesting that other mechanisms must be also partly, if not entirely, involved in producing the observed seismic anisotropy.

6.2. Relationship With Lithospheric Deformation

[41] Many studies found that the fast polarization directions of SKS waves align well with the strike of orogenic belts across the continents [*Silver*, 1996], resulting in another end-member model for explaining mantle anisotropy. The model invokes a vertically coherent deformation between the crust and mantle. Anisotropy exists largely in the lithosphere generated by the most recent significant tectonic event [*Silver*, 1996]. Here, we argue that the preference of the NW–SE fast direction in the study region is closely related to the pronounced extensional tectonic events occurring in northeast China since the late Mesozoic.

[42] Northeast China has experienced multistage contraction and extension from the Mesozoic to Cenozoic. Before the Cretaceous, northeast China was an Andean-type margin because of the subduction of the Pacific plate, and was an elevated plateau formed during the contractional Yanshanian orogeny. During 150–140 Ma, the contracted high-standing plateau started to collapse, marking a tectonic transition from contractional to extensional deformation [*Wang et al.*, 2006]. A-type granites and alkaline rocks of late Mesozoic age can be found widely in northeast China, suggesting an extensional setting in northeast China and adjacent regions at that time [*Wu et al.*, 2005]. Metamorphic core complexes show an orientation with a stretching lineation that indicates a NW–SE extension around Bohai Sea [*Allen et al.*, 1997]. This extension caused the formation of Great Xing'an volcanic belt and the Songliao basin and continued from the late Cretaceous to Tertiary. Meanwhile, a series of NE elongated rifting basins were also developed in east China.

[43] As one of the most important components of the Mesozoic-Cenozoic rift system in east China, the northeast China rift system was superimposed on a complex basement that includes Mesozoic, Paleozoic fold belts and Precambrian craton [*Tian et al.*, 1992]. The averaged fast direction in the southeast corner of the Songliao basin is N44°W, which is normal to the local trend of the basin and the Tanlu fault, and is parallel to the extensional strain direction. Recently, *Kang and Shin* [2009] investigated seismic anisotropy beneath southern Korea using ScS waves from deep earthquakes recorded at broadband stations. They applied a cross correlation based method to find the best fitting splitting parameters. A preferred NW–SE fast direction was detected in their observations, showing a striking similarity to our results in the northeast edge of NCC. On the basis of laboratory study and geological observations, in an extensional or rifting environment, the foliation plane of minerals tends to be horizontal and the stretching lineation is likely to be parallel to the extension direction. We thus infer that the observed seismic anisotropy beneath northeast China reflects the extensional deformation in the lithosphere being frozen since late Mesozoic time. Mechanism(s) responsible for the compression-to-extension transition occurring in the late Mesozoic are not well understood. While this subject is beyond the scope of this study, subduction of the oceanic Kula and Pacific plate along the eastern margin of Asian is believed to play an important role in the evolution of the east China rift system [*Tian et al.*, 1992].

6.3. Relationship With Edge and Delamination Flows

[44] At the west edge of the Songliao basin, we found some variations in the measured fast-axis direction as well as a reduced amplitude in splitting time. This edge was manifested by the NSGL at the surface by a large gradient in both gravity and topography. The underlying lithosphere beneath the NSGL is also believed to have a large gradient in thickness, with the west side being 30–50 km thicker that in the east side. *Niu* [2005] proposed that edge-driven convection might be responsible for the observed Cenozoic volcanism along the Great Xing'an Range. We also speculate that the observed scattering in fast-axis direction may result from the interactions between this small-scale flow and the asthenospheric flow associated with the APM.

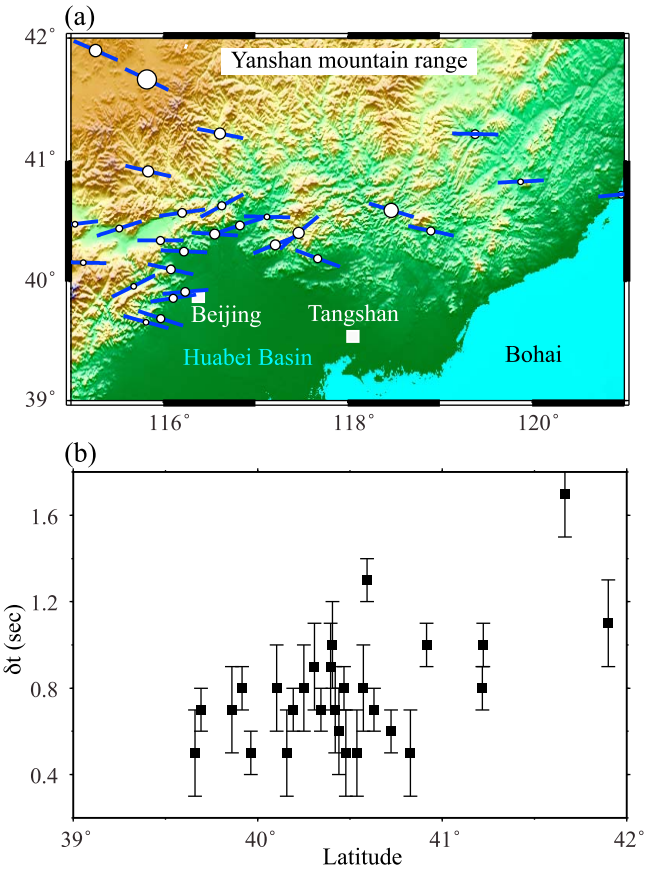

Figure 8. (a) Map showing the fast directions measured from the 29 stations located in the Yanshan mountain range and its south flank. The fast direction is roughly parallel to the E–W direction. (b) Amplitude of the delay time is plotted against the station latitude. Stations located in the north are underlain by a thick lithosphere. Note that the delay time increases toward the north, suggesting a positive correlation between the strength of the splitting signal and lithospheric thickness.

[45] We have 29 stations located within the Yanshan mountain range and its southern flank at the southwest corner of the Songliao basin. All of these stations exhibit a consistent φ in a roughly E–W direction (Figure 8a), which is distinctly different from the ~NW–SE direction observed at the rest of the stations. The direction is parallel to the strike of the Yanshan belt, thus one likely explanation of the observed seismic anisotropy is that it is due to lithospheric deformation formed during the Yanshanian orogeny in late Jurassic. Meanwhile, xenolith studies suggest that the old and depleted cratonic lithosphere in this area was removed and replaced by relatively young and undepleted mantle some time during the later Jurassic or Early Cretaceous [*Menzies et al.*, 1993; *Griffin et al.*, 1998; *Gao et al.*, 2002]. Since the xenolith sites are spatially limited, it is still unclear to what degree the lithosphere has been removed.

[46] Seismic studies indicate that the lithosphere is ~60–100 km thick beneath the Huabei plain and Bohai Sea and is ~120–200 km thick beneath the Yanshan mountain range [e.g., *Chen et al.*, 2008; *Xu and Zhao*, 2009]. It has been speculated that thinned lithosphere is due to lithosphere delamination. *Xu and Zhao* [2009] observed a high-velocity anomaly of ~100 km thick lying on the 410 km discontinuity beneath the Huabei plain. They interpreted it as a piece of the delaminated lithosphere. If this interpretation is correct, then the foundering lithosphere could induce three-dimensional flow in the asthenosphere, which may also contribute to the observed seismic anisotropy.

[47] In general, stations located at the edge of the Huabei plain have smaller splitting time than those located within the mountain range. We found a trend of increasing delay time from south to north (Figure 8b). Since the lithosphere thickens toward the north, the observed strength of the splitting signal seems to be positively correlated with the thickness of the lithosphere. Therefore we tend to argue for a lithospheric origin of the seismic anisotropy observed in this subregion.

6.4. Relationship With the Pacific Slab Rollback

[48] Beneath the Jiamusi massif, the fast polarization direction rotates in a clockwise direction from NW to NNW. Splitting times are also larger than those measured in other subregions. These features were confirmed from all of the 11 adjacent stations. The fast direction seems to be inconsistent with either the absolute plate motion or geological structures. We noticed that the stations are located right above a gap in deep seismicity at the northwestern corner of the subducting Pacific slab (Figure 6). It is unclear whether the lack of seismicity is caused by a tear within the Pacific slab or not. The Marian-Japan-Kuril trench has been migrating progressively from west to east ever since the Miocene [*Miller et al.*, 2006], resulting in an eastward rollback of the subducted Pacific plate. Global studies of mantle seismic anisotropy in subduction zones [*Long and Silver*, 2008, 2009] found that the subslab region is dominated by trench-parallel fast splitting directions, and splitting times appeared to be well correlated with the trench migration velocity. These observations agree well with lab experiment studies [e.g., *Kincaid and Griffiths*, 2003]. On the other hand, a complicated pattern of seismic anisotropy has been observed within the mantle wedge [e.g., *Anderson et al.*, 2004; *Pozgay et al.*, 2007], and it seems that slab geometry has a significant effect on the three-dimensional flow field within the mantle wedge [*Kneller and van Keken*, 2007]. If there is slab tear at the bend of the Pacific plate (Figure 6), a northwest-going flow could be induced as the Pacific slab rolls back toward the east. We speculate that this flow might be the cause of the unique anisotropy observed in this subregion.

7. Summary

[49] SKS wave splitting parameters were measured at 108 stations in northeast China using a multievent technique. The observed map of fast direction and splitting time showed clear patterns with some complexity, suggesting that a variety of mechanisms may be involved in producing the seismic anisotropy. Shear waves polarized in the NW direction are predominantly fast, which aligns well with the extensional direction of the region. Our observations also

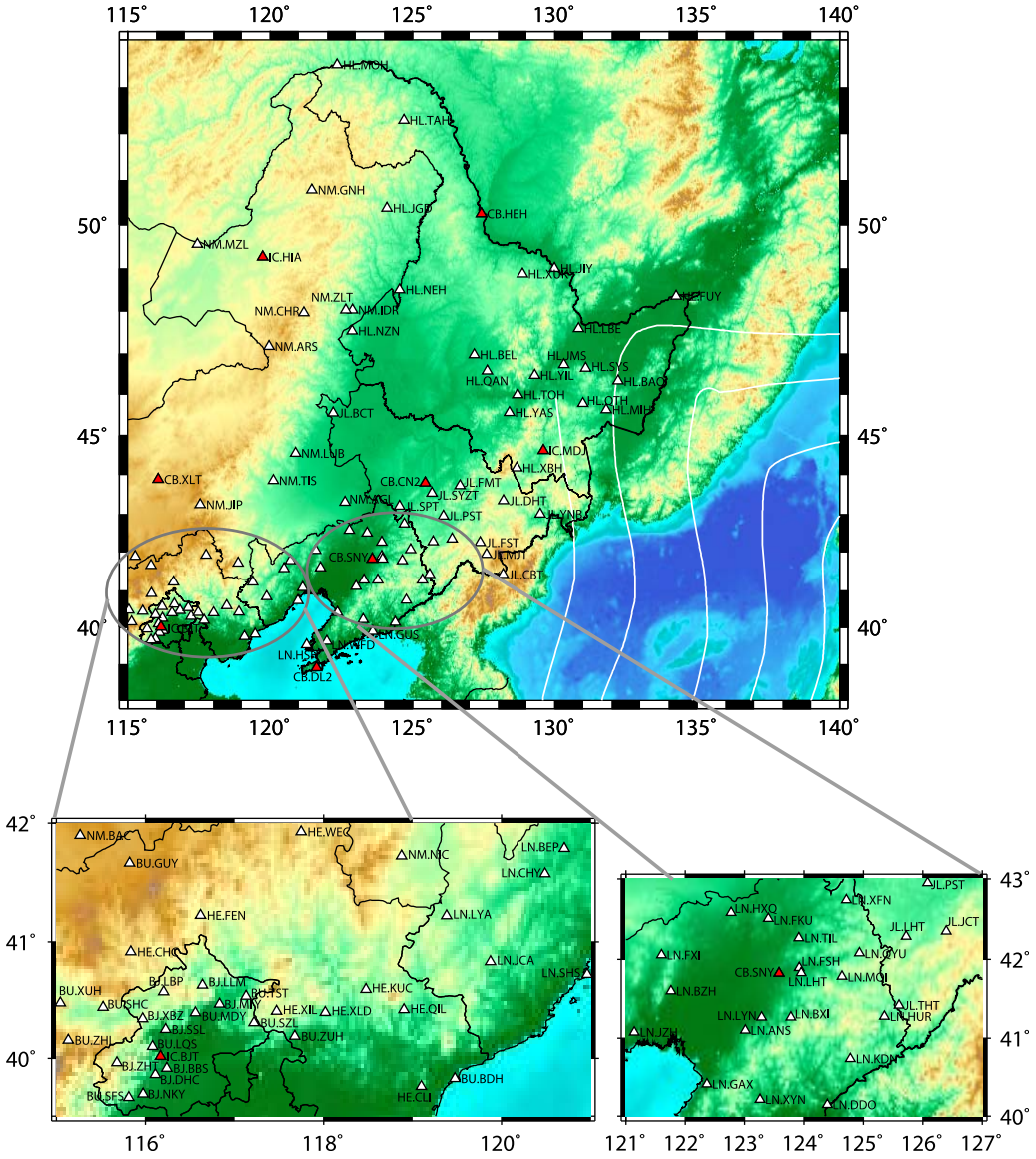

Figure A1. Seismic stations are shown with their station codes. Red and white triangles indicate stations within the GSN/national seismic network and regional seismic networks, respectively.

suggest that edge-driven flow can affect mantle deformation in both regional and local scale. Retreating of the subduction system along the east side of the study region also plays a significant role in deforming the mantle beneath northeast China.

Appendix A

[50] To better associate the anisotropy map shown in Figure 6 and the measurements listed in Table 2, here we showed the geographic location of the seismic stations with their station codes (Figure A1).

[51] **Acknowledgments.** We thank the Data Management Centre of China National Seismic Network at Institute of Geophysics, China Earthquake Administration, for providing seismic data. Critical comments from two anonymous reviewers and the Associate Editor significantly improved the quality of this paper. This work is supported by the NSFC grant 40774042, the Knowledge Innovation Program of the Chinese Academy of Sciences (J.L.), and the NSF grant EAR-063566 (F.N.).

References

Ai, Y., T. Zheng, W. Xu, and D. Dong (2003), A complex 660 km discontinuity beneath norhteast China, *Earth Planet. Sci. Lett.*, *212*, 63–71, doi:10.1016/S0012-821X(03)00266-8.

Allen, M. B., D. I. M. Macdonald, X. Zhao, S. J. Vincent, and C. Brouet-Menzies (1997), Early Cenozoic two-phase extension and late Cenozoic thermal subsidence and inversion of the Bohai Basin, northern China, *Mar. Pet. Geol.*, *14*, 951–972, doi:10.1016/S0264-8172(97)00027-5.

Anderson, M. L., G. Zandt, E. Triep, M. Fouch, and S. Beck (2004), Anisotropy and mantle flow in the Chile-Argentina subduction zone from shear wave splitting analysis, *Geophys. Res. Lett.*, *31*, L23608, doi:10.1029/2004GL020906.

Baccheschi, P., L. Margheriti, and M. S. Steckler (2007), Seismic anisotropy reveals focused mantle flow around the Calabrian slab (Southern Italy), *Geophys. Res. Lett.*, *34*, L05302, doi:10.1029/2006GL028899.

Boyd, F. R. (1989), Compositional distinction between oceanic and cratonic lithosphere, *Earth Planet. Sci. Lett.*, *96*, 15–26, doi:10.1016/0012-821X(89)90120-9.

Chang, L. J., C. Y. Wang, and Z. F. Ding (2009), Seismic anisotropy of upper mantle in eastern China, *Sci. China, Ser. D: Earth Sci.*, *52*(6), 774–783, doi:10.1007/s11430-009-0073-4.

Chen, L., W. Tao, L. Zhao, and T. Zheng (2008), Distinct lateral variation of lithospheric thickness in the northeastern North China Craton, *Earth Planet. Sci. Lett.*, *267*(1–2), 56–68, doi:10.1016/j.epsl.2007.11.024.

Deng, J. F., S. G. Su, Y. L. Niu, C. Liu, G. C. Zhao, X. G. Zhao, S. Zhou, and Z. X. Wu (2007), A possilbe model for the lithoshperic thinning of North China Craton: Evidence from the Yanshanian (Jura-Cretaceous) magmatism and tectonism, *Lithos*, *96*, 22–35, doi:10.1016/j.lithos.2006.09.009.

Fischer, K. M., M. J. Fouch, D. A. Wiens, and M. S. Boettcher (1998), Anisotropy and flow in Pacific subduction zone back-arcs, *Pure Appl. Geophys.*, *151*(2–4), 463–475, doi:10.1007/s000240050123.

Fouch, M. J., and S. Rondenay (2006), Seismic anisotropy beneath stable continental interiors, *Phys. Earth Planet. Inter.*, *158*, 292–320, doi:10.1016/j.pepi.2006.03.024.

Gao, S., R. L. Rudnick, R. W. Carlson, W. F. McDonough, and Y. S. Liu (2002), Re-Os evidence for replacement of ancient mantle lithosphere beneath the North China craton, *Earth Planet. Sci. Lett.*, *198*, 307–322, doi:10.1016/S0012-821X(02)00489-2.

Griffin, W. L., Z. Andi, S. Y. O'Reilly, and C. G. Ryan (1998), Phanerozoic evolution of the lithosphere beneath the Sino-Korean craton, in *Mantle Dynamics and Plate Interactions in East Asia*, *Geodynamics*, vol. 27, pp. 107–126, AGU, Washington, D. C.

Gripp, A. E., and R. G. Gordon (2002), Young tracks of hotspots and current plate velocities, *Geophys. J. Int.*, *150*, 321–361, doi:10.1046/j.1365-246X.2002.01627.x.

Huang, J., and D. Zhao (2006), High-resolution mantle tomography of China and surrounding regions, *J. Geophys. Res.*, *111*, B09305, doi:10.1029/2005JB004066.

Iidaka, T., and F. Niu (2001), Mantle and crust anisotropy in the eastern China region inferred from waveform splitting of SKS and PpSms, *Earth Planets Space*, *53*, 159–168.

Jenkins, G., and D. Watts (1968), *Spectral Analysis and Its Applications*, pp. 136–139, Holden-Day, San Francisco, Calif.

Kang, T.-S., and J. S. Shin (2009), Shear-wave splitting beneath southern Korea and its tectonic implication, *Tectonophysics*, *471*(3–4), 232–239, doi:10.1016/j.tecto.2009.02.021.

Kincaid, C., and R. W. Griffiths (2003), Laboratory models of the thermal volution of the mantle during rollback subduction, *Nature*, *425*, 58–62, doi:10.1038/nature01923.

Kneller, E. A., and P. E. van Keken (2007), Trench-parallel flow and seismic anisotropy in the Mariana and Andean subduction systems, *Nature*, *450*(7173), 1222–1225, doi:10.1038/nature06429.

Kusky, T. M., B. F. Windley, and M.-G. Zhai (2007), Tectonic evolution of the North China Block: From orogen to craton to orogen, *Geol. Soc. Spec. Publ.*, *280*(1), 1–34.

Li, J., Q.-F. Chen, E. Vanacore, and F. Niu (2008), Topography of the 660-km discontinuity beneath northeast China: Implications for a retrograde motion of the subducting Pacific slab, *Geophys. Res. Lett.*, *35*, L01302, doi:10.1029/2007GL031658.

Liu, K. H., S. S. Gao, Y. Gao, and J. Wu (2008), Shear wave splitting and mantle flow associated with the deflected Pacific slab beneath northeast Asia, *J. Geophys. Res.*, *113*, B01305, doi:10.1029/2007JB005178.

Long, M. D., and P. G. Silver (2008), The subduction zone flow field from seismic anisotropy: A global view, *Science*, *319*, 315–318, doi:10.1126/science.1150809.

Long, M. D., and P. G. Silver (2009), Mantle flow in subduction systems: The subslab flow field and implications for mantle dynamics, *J. Geophys. Res.*, *114*, B10312, doi:10.1029/2008JB006200.

Long, M. D., and R. D. van der Hilst (2006), Shear wave splitting from local events beneath the Ryukyu arc: Trench-parallel anisotropy in the mantle wedge, *Phys. Earth Planet. Inter.*, *155*(3–4), 300–312, doi:10.1016/j.pepi.2006.01.003.

Ma, X. Y. (1989), *Lithospheric Dynamics Map of China and Adjacent Seas and Explanatory Notes*, Geological Publ. House, Beijing.

Menzies, M. A., W.-M. Fan, and M. Zhang (1993), Paleozoic and Cenozoic lithoprobes and the loss of >120 km of Archean lithosphere, Sino-Korean craton, China, in *Magmatic Processes and Plate Tectonics*, edited by H. M. Prichard et al., pp. 71–81, Geol. Soc., London.

Miller, M. S., B. L. N. Kennett, and V. G. Toy (2006), Spatial and temporal evolution of the subducting Pacific plate structure along the western Pacific margin, *J. Geophys. Res.*, *111*, B02401, doi:10.1029/2005JB003705.

Niu, F., T. Bravo, G. Pavlis, F. Vernon, and H. Rendon (2007), Receiver function study of the crustal structure of the southeastern Caribbean plate boundary and Venezuela, *J. Geophys. Res.*, *112*, B11308, doi:10.1029/2006JB004802.

Niu, Y. (2005), Generation and evolution of basaltic magmas: Some basic concepts and a new view on the origin of Mesozoic-Cenozoic basaltic volcanism in eastern China, *Geol. J. China Univ.*, *11*, 9–46.

Niu, F., and J. Li (2010), Component azimuths of the CEArray stations estimated from P-wave particle motion, *Earthquake Science*, in press.

Pozgay, S. H., D. A. Wiens, J. A. Conder, H. Shiobara, and H. Sugioka (2007), Complex mantle flow in the mariana subduction system: evidence from shear wave splitting, *Geophys. J. Int.*, *170*, 371–386.

Ren, J., K. Tamaki, S. Li, and J. Li (2002), Late Mesozoic and Cenozoic rifting and its dynamic setting in eastern China and adjacent areas, *Tectonophysics*, *344*, 175–205, doi:10.1016/S0040-1951(01)00271-2.

Rumpker, G., and P. G. Silver (1998), Apparent shear-wave splitting parameters in the presence of vertically varying anisotropy, *Geophys. J. Int.*, *135*, 790–800, doi:10.1046/j.1365-246X.1998.00660.x.

Savage, M. K. (1999), Seismic anisotropy and mantle deformation: What have we learned from shear wave splitting?, *Rev. Geophys.*, *37*(1), 65–106, doi:10.1029/98RG02075.

Savage, M. K., and P. G. Silver (1993), Mantle deformation and tectonics: Constraints from seismic anisotropy in western United States, *Phys. Earth Planet. Inter.*, *78*, 207–227, doi:10.1016/0031-9201(93)90156-4.

Schulte-Pelkum, V., and D. K. Blackman (2003), A synthesis of seismic P and S anisotropy, *Geophys. J. Int.*, *154*(1), 166–178, doi:10.1046/j.1365-246X.2003.01951.x.

Sengör, A. M., and B. A. Natalin (1996), Palaeotectonics of Asia: Fragments of a synthesis, in *The Tectonic Evolution of Asia*, edited by A. Yin and T. M. Harrison, pp. 486–640, Cambridge Univ. Press, Cambridge.

Silver, P. G. (1996), Seismic anisotropy beneath the continents: Probing the depths of geology, *Annu. Rev. Earth Planet. Sci.*, *24*, 385–432, doi:10.1146/annurev.earth.24.1.385.

Silver, P. G., and W. W. Chan (1991), Shear wave splitting and subcontinental mantle deformation, *J. Geophys. Res.*, *96*(B10), 16,429–16,454, doi:10.1029/91JB00899.

Silver, P. G., and M. K. Savage (1994), The interpretation of shear-wave splitting parameters in the presence of two anisotropic layers, *Geophys. J. Int.*, *119*, 949–963, doi:10.1111/j.1365-246X.1994.tb04027.x.

Smith, G. P., D. A. Wiens, K. M. Fischer, L. M. Dorman, S. C. Webb, and J. A. Hildebrand (2001), A complex pattern of mantle flow in the Lau backarc, *Science*, *292*(5517), 713–716, doi:10.1126/science.1058763.

Tian, B. F., et al. (2008), Crustal anisotropy of Taihangshan mountain range in north China inferred from receiver functions (in Chinese), *Chin. J. Geophys.*, *51*(5), 1459–1467.

Tian, Z.-Y., P. Han, and K.-D. Xu (1992), The Mesozoic-Cenozoic east China rift system, *Tectonophysics*, *208*(1–3), 341–363, doi:10.1016/0040-1951(92)90354-9.

Wang, D. (1986), Volcanic rocks of Mesozoic-Cenozoic rifting in eastern China (in Chinese), *Bull. Changchun Coll. Geol.*, *3*, 18–32.

Wang, F., X.-H. Zhou, L.-C. Zhang, J.-F. Ying, Y.-T. Zhang, F.-Y. Wu, and R.-X. Zhu (2006), Late Mesozoic volcanism in the Great Xing'an Range (NE China): Timing and implications for the dynamic setting of NE Asia, *Earth Planet. Sci. Lett.*, *251*(1–2), 179–198, doi:10.1016/j.epsl.2006.09.007.

Wu, F. Y., D. Y. Sun, H. M. Li, and X. L. Wang (2001), The nature of basement beneath the songliao basin in NE China: Geochemical and isotopic constraints, *Phys. Chem. Earth*, *26*, 793–803, doi:10.1016/S1464-1895(01)00128-4.

Wu, F.-Y., J.-Q. Lin, S. A. Wilde, X. O. Zhang, and J.-H. Yang (2005), Nature and significance of the early Cretaceous giant igneous event in eastern China, *Earth Planet. Sci. Lett.*, *233*(1–2), 103–119, doi:10.1016/j.epsl.2005.02.019.

Wu, J., Y. Gao, Y. Chen, and J. Huang (2007), Seismic anisotropy in the crust in northwestern capital area of China (in Chinese), *Chin. J. Geophys.*, *50*(1), 209–220.

Xu, P. F., and D. P. Zhao (2009), Upper-mantle velocity structure beneath the North China Craton: Implications for lithospheric thinning, *Geophys. J. Int.*, *177*, 1279–1283, doi:10.1111/j.1365-246X.2009.04120.x.

Xu, Y.-G. (2007), Diachronous lithospheric thinning of the North China Craton and formation of the Daxin'anling-Taihangshan gravity lineament, *Lithos*, *96*(1–2), 281–298, doi:10.1016/j.lithos.2006.09.013.

Zhang, S., and S.-i. Karato (1995), Lattice preferred orientation of olivine aggregates deformed in simple shear, *Nature*, *375*(6534), 774–777, doi:10.1038/375774a0.

Zhao, D., S. Maruyama, and S. Omori (2007a), Mantle dynamics of Western Pacific and East Asia: Insight from seismic tomography and mineral physics, *Gondwana Res.*, *11*(1–2), 120–131, doi:10.1016/j.gr.2006.06.006.

Zhao, L., T. Zheng, L. Chen, and Q. Tang (2007b), Shear wave splitting in eastern and central China: Implications for upper mantle deformation beneath continental margin, *Phys. Earth Planet. Inter.*, *162*, 73–84, doi:10.1016/j.pepi.2007.03.004.

Zheng, X. F., Z. X. Yao, J. H. Liang, and J. Zheng (2010), The role played and opportunities provided by IGP DMC of China National Seismic Network in Wenchuan earthquake disaster relief and researches, *Bull. Seismol. Soc. Am.*, *100*, 2866–2872, doi:10.1785/0120090257.

J. Li, Key Laboratory of the Earth's Deep Interior, Institute of Geology and Geophysics, Chinese Academy of Sciences, Beijing 100029, China.

F. Niu, Department of Earth Science, Rice University, Houston, TX 77005, USA.